International Journal for Housing Science and Its Applications
Publish August 4, 2025. Volume 46, Issue 3 Pages 2414-2435

https://doi.org/10.70517/ijhsa463202

Multi-objective optimization of demand response for central air conditioning systems: enhancing energy flexibility in libraries

Tianhui Yang[1], Zehua Liu[1,*], Chen Yuan[1], Dan Xie[1] and Bin Wang[1]
[1] School of Civil Engineering, University of South China, Hengyang, Hunan, 421001, China
Corresponding authors: (e-mail: 19925713607@163.com).

Abstract Heating, ventilation, and air-conditioning (HVAC) systems play a pivotal role in demand response (DR) by enabling load modulation to enhance energy flexibility. However, traditional strategies often optimize only a single variable—such as indoor temperature or chilled water temperature—limiting coordinated system control. In addition, the influence of dynamic occupant distribution on building energy performance and flexibility is rarely considered, especially in high-occupancy spaces like libraries.To address these limitations, this study proposes a multidimensional synergistic control strategy that simultaneously optimizes indoor temperature setpoints, chilled water supply temperature, and fresh air unit operation to enhance energy efficiency and DR performance. A TRNSYS-based simulation model of a university library in Hunan Province was developed to evaluate the strategy. Key performance indicators included peak load reduction, energy savings, and indoor thermal comfort, benchmarked against a baseline control strategy. The impact of occupant seating patterns on control effectiveness was also examined.Results show that, compared to the baseline strategy (ST1), the proposed strategy (ST6) reduces energy consumption during DR periods by 34.3%, daily energy use by 14.92%, and electricity costs by 20.00%. Concentrated occupant distribution further improves load regulation and system efficiency. This study demonstrates that integrating occupant behavior into multidimensional HVAC control offers a scalable and effective solution for enhancing DR capacity, building energy performance, and operational cost savings.

Index Terms Multi-dimensional Coordinated Optimization, Demand Response, Fresh Air Flexibility, Multi-objective optimization control, differential occupancy

I. Introduction

The rapid development of society and the economy has exacerbated the imbalance between electricity supply and demand, posing significant challenges to grid stability and energy efficiency. Building energy consumption constitutes a major portion of the overall electricity load, among which heating, ventilation, and air conditioning (HVAC) systems account for approximately 48% of the total energy consumption in public buildings. This issue becomes even more critical during summer, when rising ambient temperatures substantially increase cooling demand, making HVAC systems the primary driver of peak electricity consumption. Therefore, optimizing the operation of HVAC systems is essential for alleviating supply-demand imbalances and improving energy efficiency.

Demand Response (DR) strategies, as an effective demand-side management tool, aim to guide consumers to adjust their electricity usage patterns via flexible control mechanisms, thereby reducing loads during peak periods and achieving optimal power consumption. Currently, two types of DR strategies are commonly adopted in HVAC systems: load shifting and load shedding[1]. Load shifting refers to the transfer of all or part of the peak load to off-peak periods by utilizing energy storage systems or the thermal inertia of buildings [2]. Load shedding, on the other hand, directly reduces power consumption through end-use control[3], source-side regulation [4] , or ventilation system adjustments [5].

In terms of terminal control, studies have shown that increasing indoor temperature by 1°C during DR periods can reduce HVAC energy consumption by approximately 10% [6]. Both experimental and simulation studies [7]have demonstrated that, compared to fixed temperature setpoints, dynamic adjustments can reduce energy consumption by 2.8% and operating costs by 3.73%, while maintaining thermal comfort within a temperature deviation of 1–2°C. Moreover, combining pre-cooling strategies with optimization algorithms can reduce peak loads by up to 80%, while still meeting thermal comfort and time-of-use (TOU) pricing constraints [8]. Li et al.[9] employed a neural network-optimized reinforcement learning algorithm to enhance robustness and used TOU pricing to control thermostats during DR periods, achieving a 9.17% reduction in operating costs compared to fixed temperature settings. Li et al.

[10] also proposed an improved HVAC indoor temperature prediction strategy that simplifies computation for real-time control. However, their method did not support dynamic adjustment of indoor temperature setpoints.Although these studies emphasize indoor temperature control, such strategies may reduce occupant comfort—particularly in large buildings or residential environments—where temperature adjustments may result in overheating or overcooling in different zones. In addition, load reduction capacity is often constrained by Predicted Mean Vote (PMV) limits. While many centralized HVAC systems are equipped with automatic control devices at the design stage, in practice, a considerable number of these systems have degraded or become nonfunctional. Even in functional systems, conservative control parameters—such as low proportional gain and high integral gain in PI control—are typically configured during initial commissioning to ensure system stability [11], which can result in a time lag of several hours from temperature setpoint adjustment to noticeable changes in chiller energy consumption. This delayed response clearly falls short of the rapid adjustment requirements of modern DR programs, especially during peak grid demand.

In source-side control, one commonly adopted method is directly turning off one or more chillers during peak demand periods to quickly reduce system power consumption. However, this may lead to hydraulic imbalance, uneven cooling distribution, and non-uniform temperature increases [12]. In contrast, optimizing the chilled water supply temperature can address these issues. This approach is recognized as one of the most effective energy-saving strategies, capable of reducing base load energy consumption by up to 14.2% [13]. Ran et al. [14] developed a virtual flowmeter model and a self-regulating flow monitoring system to estimate chilled water flow in each AHU in real time, ensuring balanced distribution among units and reducing power demand during DR events. Dai et al.[15] proposed an event-driven control mechanism that adjusts AHU valve positions based on indoor temperature deviation thresholds, enabling uniform temperature rise while minimizing valve actuator movement. A feedback control strategy based on adaptive utility functions was also introduced, incorporating both global and local cooling demand allocators to dynamically reset chilled water flow and air supply volume across different zones, thereby addressing the issue of uneven temperature increase during DR events [16]. Compared to direct on-off control, adjusting chilled water supply temperature is a more gradual approach, avoiding frequent cycling of chillers and their associated pumps or cooling towers, which can otherwise impair system performance and reduce equipment lifespan. However, this approach still relies on modulating cooling capacity and may lead to internal energy offset by other devices (e.g., pumps, fans), potentially weakening the intended load reduction.

In ventilation-side management, existing studies have explored supply air temperature control, static pressure reduction, and fan operation optimization. For instance, reinforcement learning has been applied to optimize dynamic static pressure control, reducing fan energy consumption by 38.5% and electricity costs by 18.5% compared to fixed settings. Vand et al. investigated a CO_2-based feedback control strategy for educational offices in cold climates, showing that its energy and cost-saving potential increases with occupant density, as CO_2 concentrations fluctuate between 800–1200 ppm [17]. Rotger et al. [18] found that demand-controlled ventilation (DCV) can achieve up to 2% peak-period electricity savings. The varying DR potential of HVAC systems is partly due to current research focusing primarily on sensible load management, while latent load contributions are often overlooked. Ma et al. [19] analyzed the impact of latent cooling loads in four representative humid climate zones, showing that ventilation control could provide 30%–40% flexibility in total cooling demand, with latent loads accounting for 56%–66.4% of this flexibility. Luo et al. [20] proposed a CO_2-based ventilation adjustment strategy for office buildings, demonstrating that due to its fast response and low inertia, CO_2 feedback control is highly suitable for short-term DR applications, achieving an average 34% reduction in ventilation load during summer peak hours.

In summary, existing research on HVAC-related DR strategies predominantly focuses on single-variable control, such as temperature, cooling source, or ventilation adjustments, and lacks practical implementations of integrated control schemes. For instance, temperature and humidity joint control (T&H) strategies have been proposed to simultaneously manage sensible and latent loads, achieving a 29.15% reduction in electricity consumption and a 46.11% decrease in daily operational costs during DR periods [21]. Wang et al. [22]introduced a coordinated control strategy that adjusts both chilled water supply temperature and indoor temperature setpoints to enhance power response speed while balancing cooling demand. This approach synchronizes supply and demand from the source, improving response time and reducing internal energy offset. However, the feasibility and real-world effectiveness of such methods still require further experimental validation. Yuan et al. [23] proposed a T&H control strategy that synchronously adjusts supply air temperature and chilled water temperature to manage both sensible and latent loads. Compared to traditional approaches, this method improved energy savings to 39.0% and peak load reduction to 37.1%, particularly in high-latent-load scenarios. These findings indicate that integrated control strategies outperform conventional approaches in terms of energy savings, responsiveness, and occupant comfort, and are especially well-suited for modern buildings participating in DR programs.

Nevertheless, existing integrated strategies often overlook indoor environmental quality and human thermal comfort in their control logic. Therefore, incorporating the fresh air system into DR strategies represents a promising direction for optimizing overall system performance.

These studies collectively indicate that a wide range of DR strategies related to load shifting and load shedding have been explored in buildings and HVAC systems. However, there remain the following key research gaps:

(1) Limited control dimensions and insufficient response flexibility:

Most existing DR strategies for HVAC systems focus on single-variable control, such as adjusting indoor temperature setpoints or chilled water supply temperatures. These approaches lack coordination among the cooling source, terminal load, and air-side subsystems. As a result, they often exhibit limited flexibility in load regulation and may lead to internal energy offset due to compensatory operation of other components such as pumps and fans, thereby reducing the net load reduction potential.

(2) Lack of multi-parameter coordinated control strategies that incorporate fresh air systems:

The fresh air system plays a crucial role in latent load regulation, ventilation demand adjustment, and rapid DR response. However, it is often oversimplified or neglected in existing DR strategies. Although temperature and humidity (T&H) joint control methods consider latent load, they generally underutilize the potential of fresh air system regulation and may involve high implementation complexity. Therefore, there is an urgent need to develop an integrated control strategy that combines fresh air system operation, chilled water supply temperature, and indoor temperature setpoint adjustments, in order to enhance the overall energy efficiency and DR performance of HVAC systems.

To address the existing limitations in energy management, this study proposes an integrated DR framework for a university library in Hengyang, which adopts a hierarchical control strategy across multiple subsystems. This approach enables coordinated optimization of terminal unit operation, cooling source scheduling, and fresh air regulation to improve energy efficiency and indoor comfort. The optimization framework employs the Non-dominated Sorting Genetic Algorithm II (NSGA-II)[24], a well-established multi-objective optimization method in building energy studies, known for effectively handling nonlinear trade-offs. The proposed method explicitly accounts for subsystem coupling effects, including: Chilled water temperature regulation, which influences the dehumidification capacity of terminal units; Variable-frequency fresh air control, dynamically adjusting ventilation rates based on real-time CO_2 concentration to balance indoor air quality and cooling loads. By integrating these strategies, the framework enhances system-wide energy efficiency while ensuring occupant comfort.

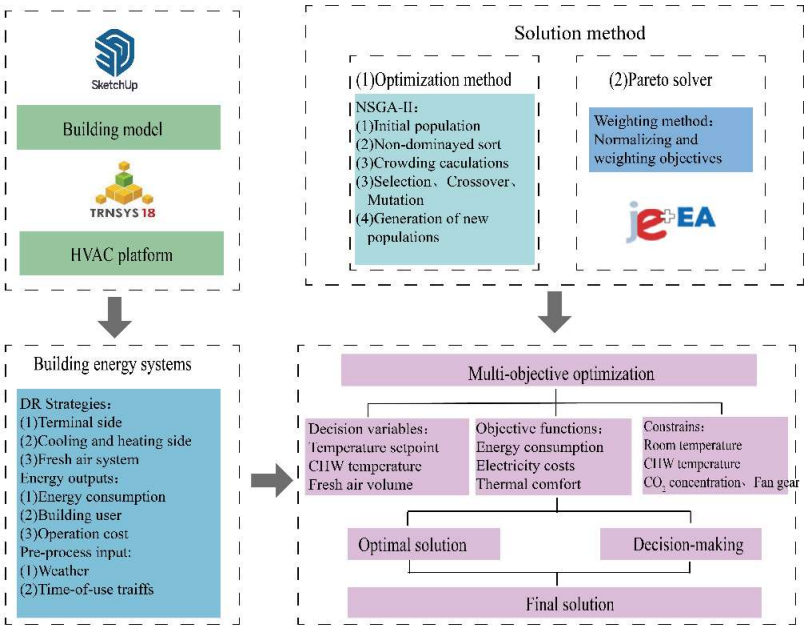

Figure 1: Multidimensional Collaborative Load Optimization Framework

The structure of this paper is organized as follows: Section 2 presents the framework for multidimensional collaborative load optimization. Section 3 describes the energy consumption characteristics of the university library and the modeling approach for the HVAC. Section 4 introduces the DR based multi-objective optimization model and which is applied to the library as a case study considering energy flexibility, economic efficiency, and human thermal

comfort. Section 5 analyzed the performance of the multidimensional optimization strategy which is compared with a single optimization method in terms of peak demand, thermal comfort, and energy savings. Section 6 discusses the strengths and limitations of the proposed approach, followed by the conclusions. Section 7 provides a summary of the conclusions.

II. Methodology

This study presents a multidimensional collaborative load optimization framework for HVAC demand response, which primarily consists of two key components: (1) a simulation model of the building and its air-conditioning system, and (2) a multi-objective optimization model as shown in Figure 1. The design parameters govern multiple dimensions through a synergistic optimization approach to achieve optimal operation of the air-conditioning system.

III. Building and HVAC system simulation model

This section may be divided by subheadings. It should provide a concise and precise description of the experimental results, their interpretation, as well as the experimental conclusions that can be drawn.

III. A. Building information and cooling load calculation

This study focuses on a university library located in Hengyang City, which consists of two subterranean levels and ten aboveground levels, encompassing a total floor area of 39,552.5 m² and a height of 47.50 m. The central air-conditioning system serves the first through eighth floors, covering an area of 26,465 m². The first floor features a spacious hall, while the second through eighth floors function as reading rooms. The second floor has a height of 6.3 meters, whereas the remaining floors each have a height of 4.5 meters The window-to-wall ratios for the east, south, west, and north facades are 0.54, 0.55, 0.51, and 0.54, respectively. In contrast to conventional buildings, university libraries generally remain closed during the winter and summer seasons. The architectural design drawings of the library indicate that SketchUp is utilized to create a three-dimensional model of the library, as illustrated in Figure 2. The layout distribution is presented in Figure 3, while the materials used for the enclosure structure are detailed in Table 1.

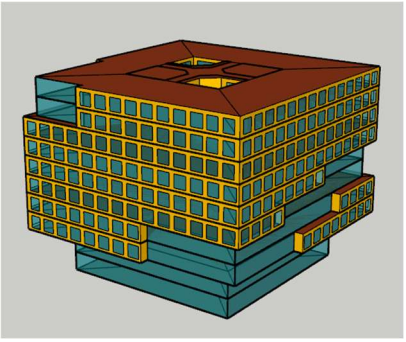

Figure 2: 3D model diagram

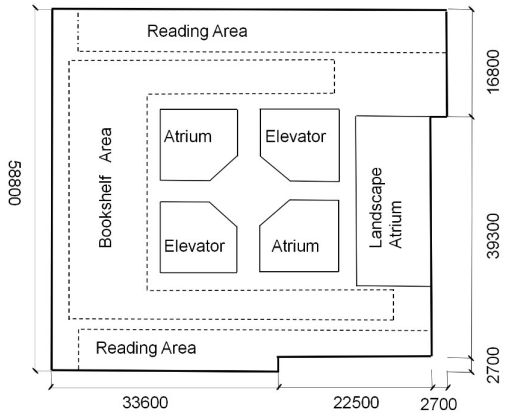

Figure 3: Standard floor plan layout diagram

Table 1: Envelope Structure Material Table

Envelope	Fabric	Heat transfer coeffi-cient/(w·(m2·K)-1)
External wall	Mixed mortar (20 mm) + sintered shale porous brick (200 mm) + cement mortar (20 mm) + rock wool board (40 mm) + anti-cracking polymer mortar (5 mm)	0.46
Roof	Mixed mortar (20 mm) + reinforced concrete (120 mm) + cement mortar (20 mm) + extruded polystyrene board (60 mm) + fine stone concrete (70 mm)	0.488
Floor	Cement mortar (20 mm) + reinforced concrete (120 mm) + cement mortar (20 mm)	0.688
Interior wall	Cement mortar (20 mm) + sintered shale porous brick (200 mm) + Cement mortar (20 mm)	1.67
External window	Aluminum alloy with a solar heat gain coefficient of 0.29 and a visible light transmission ratio of 0.62.	2.39

Indoor heat gain primarily arises from three sources: occupants, equipment, and lighting. The relevant parameters are established in accordance with the 'Energy Saving Design Code for Public Buildings '[25].The seating capacities for the first to eighth floors are 25, 254, 456, 424, 400, 336, 460, and 296, respectively. The seating capacities for the first to eighth floors are 25, 254, 456, 424, 400, 336, 460, and 296, respectively. The maximum heat dissipation rates are 9 W/m² for lighting and 15 W/m² for equipment. The usage schedules for occupants, lighting, and electrical appliances are illustrated in Figure 4. The variation trends of personnel, equipment, and lighting usage provide valuable insights into energy optimization opportunities. The key observations are as follows:

(1) Bimodal Usage Patterns: In work and study environments, a clear "bimodal" usage pattern emerges, with two distinct peaks in activity: one in the morning (9:00-12:00) and another in the afternoon (14:00-18:00). These peaks correspond to intensive work or study periods, where personnel, equipment, and lighting are heavily utilized, reflecting sustained productivity throughout the day.

(2) Lunch Break Decline: During the lunch break (12:00-14:00), a noticeable reduction in personnel and equipment usage is observed, signaling a shift to rest periods. Despite this, lighting usage remains relatively high, likely due to baseline illumination being maintained even when occupancy is lower. This presents an opportunity for energy optimization by adjusting lighting levels according to actual occupancy.

(3) Evening and Nighttime Decline: From 18:00-24:00, usage gradually decreases. Between 18:00-21:00, personnel, equipment, and lighting usage decline gradually, likely reflecting overtime, night shifts, or reduced activity. However, between 21:00-24:00, usage drops significantly, approaching zero, indicating that the space is largely inactive. This period highlights opportunities to optimize lighting and equipment operation strategies to reduce energy consumption during these hours.

(4) Late-Night Hours: During the late-night period (00:00-06:00), usage is minimal, with personnel absent, most equipment turned off, and lighting usage close to zero, except for possibly some safety lighting. The space is essentially in a static state during these hours, providing an ideal opportunity to further optimize equipment standby modes and minimize unnecessary energy consumption.

These trends suggest several areas where energy-saving measures can be effectively implemented, particularly through more responsive lighting and equipment management strategies based on real-time occupancy patterns.

The daily attendance data of the spring 2024 semester is presented in Figure 5, with the study spanning from June 1 to July 15. This period covers both the summer peak electricity demand period and the final exam preparation phase. The data reveal a distinct temporal pattern in peak attendance. From early June to the final exam week (June 24-30), the daily average attendance steadily increased, reaching a maximum single-day peak of 2,793 visitors. After July 1, as the summer vacation approached and exam schedules became more dispersed, daily attendance dropped sharply by 42.6%, with a minimum recorded value of 1,249 visitors. Based on these fluctuations, attendance levels were subsequently classified into four categories for analysis: high-load days (>2318 visitors, 13 days), medium-high load days (1756-2318 visitors, 14 days), medium-low load days (1249-1756 visitors, 9 days), and low-load days (<1249 visitors, 5 days). This classification facilitates a comparative analysis of how dynamic changes in occupant density impact the cooling load. As shown in Figure 6, every 10% reduction in attendance results in a decrease of 3.414 kWh/m² in the air-conditioning cooling load.

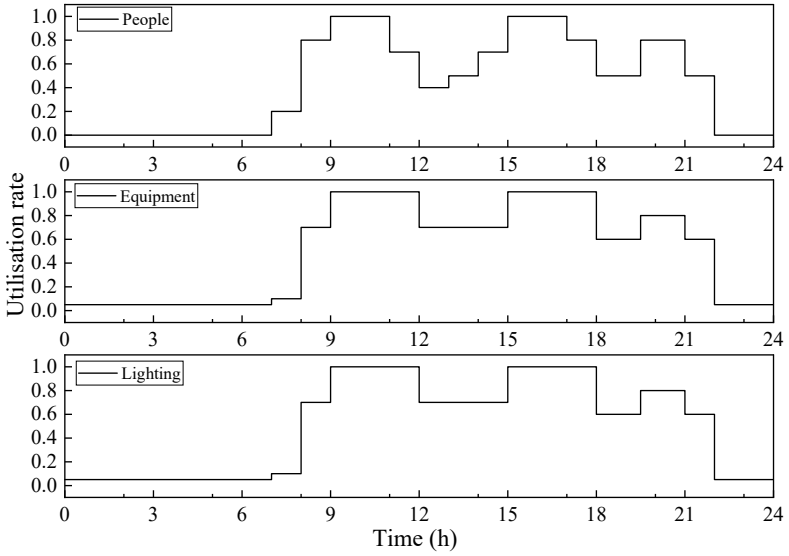

Figure 4: 3D model diagram

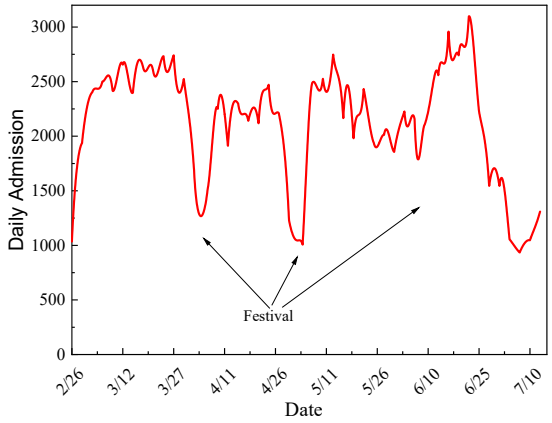

Figure 5: Daily library attendance

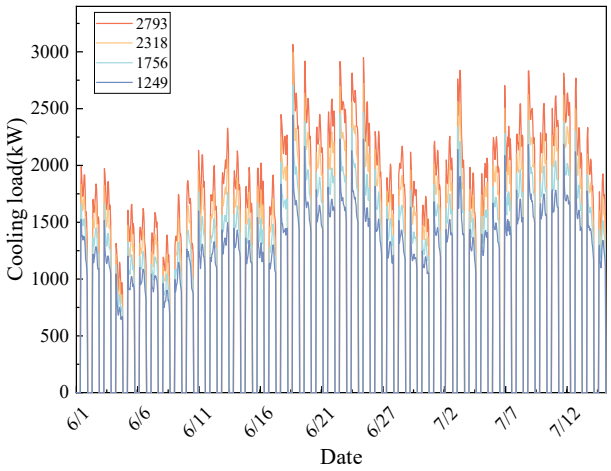

Figure 6: Standard floor plan layout diagram

III. B. HVAC system modeling

The cooling source for the library's air-conditioning system consists of two chiller units: a magnetic levitation unit with a cooling capacity of 870 kW and a centrifugal chiller unit with a cooling capacity of 2,450 kW. The chilled water inlet and outlet temperatures are 7°C and 12°C, respectively. The system includes two chilled water pumps and two

cooling water pumps. The smaller chilled water pump has a flow rate of 170 m³/h, while the larger one has a flow rate of 450 m³/h. The smaller cooling water pump operates at a flow rate of 180 m³/h, and the larger cooling water pump has a flow rate of 580 m³/h. Additionally, the cooling system also features two cooling towers, which are characterized by relatively low and stable fan operating power compared to the chiller units and pump. Therefore, this paper assumes their power to be constant and equal to the rated value.

III. B. 1) Chiller

The mathematical model of the chiller is represented as a multivariate polynomial model [26]in the following format:

$$\begin{aligned} \mathrm{COP} = {} & a_1 + a_2 Q + a_3 T_{ei} + a_4 T_{ci} + a_5 Q^2 + a_6 T_{ei}^2 \\ & + a_7 T_{ci}^2 + a_8 Q T_{ei} + a_9 Q T_{ci} + a_{10} T_{ei} T_{ci} \end{aligned} \tag{1}$$

The part-load performance of the chiller can be represented by the curve using the following equation:

$$\begin{aligned} PLCC = {} & C_0 + C_1 \times PLR + C_2 \times (PLR)^2 \\ & + C_3 \times (PLR)^3 \end{aligned} \tag{2}$$

The operating power of the chiller at various load rates is calculated as follows:

$$P_{chiller} = \frac{Q}{COP} PLCC \tag{3}$$

where, Pchiller is the power consumption of the chiller,kW; Q is the cooling capacity,kW; Tci is cooling water inlet temperature,℃; Tei is chilled water supply temperature,℃; COP is the chiller performance coefficient;a1~a10 are coefficients; PLCC is the part-load correction factor,PLR Indicates part load factor, c0~ c3 are partial load fitting coefficients.

The least squares method was employed to fit the chiller model, and the corresponding fitting results are presented in Table .

Table 2: Parameter identification results of chiller performance

Fitting coefficients	Magnetic Levitation Unit	Centrifuge unit
α1	7.9064	-17.8768
α2	-11.6178	37.7926
α3	0.3693	-0.8074
α4	-0.1227	0.1885
α5	5.5865	-18.0858
α6	0.0047	-0.0093
α7	0.0007	-0.0003
α8	-0.2941	0.8054
α9	0.0726	-0.2235
α10	-0.0034	0.0047
c0	-0.0002	-0.0031
c1	0.4142	1.2386
c2	0.3693	-0.8733
c3	0.2165	0.6347
R2	0.9931	0.992
RMSE	0.0133	0.0038

III. B. 2) Pump

The energy consumption of a water pump is expressed as a single-valued function of the flow rate, with the frequency conversion regulated by a control signal during operation. This control signal is determined d by the ratio of the desired flow rate to the rated flow rate. The pump characteristics are described in Eq. (4).

$$P_{pump} = \mathrm{P}_{rated} \left(b_0 + b_1 \frac{m}{m_{rated}} + b_2 \left(\frac{m}{m_{rated}} \right)^2 + b_3 \left(\frac{m}{m_{rated}} \right)^3 \right) \tag{4}$$

Where, Ppump is the pump power, kW;b0~ b3is the polynomial coefficient; m represents the pump flow rate, m3/h; mrated is the rated flow rate of the pump,m3/h;Prated is the rated power of the pump,kW.

The results of fitting the chilled and cooling water pumps using the least squares method are shown in Table 3.

Table 3: Parameter identification results of chilled water and cooling water pumps

Fitting coefficients	Chilled water pump	Cooling water pump
b0	0.5881	0.4337
b1	0.4374	0.9153
b2	-0.1053	-0.4033
b3	0.0793	0.0565
R2	0.9841	0.9689
RMSE	0.2509	0.4758

III. B. 3) Air-handling units

The mathematical model of air-handling units is presented in equations(5)~(8):

$$m_{water} = \dot{m}_{air}(1 - f_{bypass})(\omega_{air,\,out} - \omega_{air,\,out}) \tag{5}$$

where, mwater is the condensate flow rate through the coil, kg/h,ṁair is the total airflow rate through the coil, kg/h;fbypassis the proportion of air passing through the bypass coil ranges from 0 to 1; ωair,in, ωair,out represents the absolute humidity of the air before it enters the coil and after it exits the coil, respectively, kg(H20) /kg(air).

The energy transferred from air to water is:

$$Q_{fluid} = \dot{m}_{air}(1 - f_{bypass})(h_{air,\,in} - h_{air,\,out}) - \dot{m}_{cond}h_{cond} \tag{6}$$

where, Qwater is the heat transferred from air to water, kg/h,hair,in, hair,out represents the enthalpy of air inlet and outlet, kj/k, respectively; h_{cond} is the enthalpy of condensate entering the coil,kj/kg; ṁcond is flow rate of condensate through the coil, kg/h;hcond is entering enthalpy of the condensate in the coil,kJ/kg.

The chilled water outlet temperature is:

$$T_{water,\,out} = T_{water,\,in} + \frac{Q_{water}}{m_{water}Cp_{water}} \tag{7}$$

where, Twater,in,Twater,out represent the condensate inlet and outlet temperatures, respectively. CPwater is the specific heat of water,kj/(kg·k)。

The enthalpy of the mixed air is:

$$h_{air,\,mix} = (1 - f_{bypass})h_{air,\,out} + f_{bypass}h_{air,\,in} \tag{8}$$

III. B. 4) Modeling of Carbon Dioxide Concentration

The modelling of the carbon dioxide concentration in the room is described below:

$$\frac{dC_{node}}{dt} = n\varepsilon C_{sup} - n\varepsilon C_{ret} + G_{pers} + G_{misc} \tag{9}$$

$$G_{pers} = \frac{g_{pers}}{V}10^6\ ppm \tag{10}$$

$$G_{misc} = \frac{g_{misc}}{V}10^6\ ppm \tag{11}$$

where, n is air changes quantified as 1; Csup、Cret represent CO2 concentration for supply and return air measured in parts per million (ppm), respectively. Cnode is CO2 concentration of room. gpers is indoor personnel CO2 production rate expressed in cubic meters per hour (m³/h), which correlates with the personnel rate outlined in Section 2.2. Gpers is total CO2 production by indoor personnel. gmisc is additional carbon dioxide concentration from other sources by indoor personnel. Gmisc is total additional carbon dioxide concentration from other source. Vis volume of the room expressed in cubic meters (m³). ε is ventilation efficiency, assumed to be 1.

III. B. 5) Energy Modeling of Fresh Air Units

The airflow produced by the fan demonstrates a linear relationship with the control signal. The energy consumption can be described by the following mathematical model:

$$P_{fan} = P_{fanrated}(d_0 + d_1\gamma + d_2\gamma^2 + d_3\gamma^3) \tag{12}$$

$$\gamma = \frac{\dot{m}}{\dot{m}_{rated}} \tag{13}$$

where, Pfan,Pfanrated represent the operating power and rated power of the fan, kJ/h, respectively. d1~ d3 are he polynomial coefficients,γ is the fan control signal,ṁfan、ṁrated represent the fan mass flow rate and the rated mass flow rate, kg/h, respectively.

III. B. 6) Performance evaluation metrics

To quantify the system performance under the multidimensional collaborative strategy, energy savings, peak load reduction, PMV (Predicted Mean Vote), and Operating Cost were used as evaluation metrics.

Energy savings

The energy savings represent the percentage reduction in daily energy consumption due to the demand response (DR) strategy, as shown in the equation.

$$E_{saving} = \frac{E_{(before,\,DR)} - E_{(after,\,DR)}}{E_{(before,\,DR)}} \tag{14}$$

where E(before,DR) and E(after,DR) represent the daily energy consumption before and after the implementation of the DR strategy, respectively, kW·h.

Peak load sheding

Peak load reduction refers to the percentage decrease in peak power load following a DR event, as shown in the equation.

$$P_{peakshedding} = \frac{P_{(before,\,DR)} - P_{(after,\,DR)}}{P_{(before,\,DR)}} \tag{15}$$

PMV(Predicted Mean Vote)

PMV is an index used to predict an individual's average vote on a 7-point thermal sensation scale, where “+3” represents extremely hot and “-3” represents extremely cold [27]. It quantifies the deviation between the actual heat flux of the human body in a given environment and the optimal comfort heat flux, as shown in Equation (3).

$$\begin{aligned} PMV = {} & [0.303\times exp(-0.036\times M)+0.028]\times\{M-W-3.05\times[5.733-0.007\times(M-W)-p_a] \\ & -0.42\times(M-W-58.2)-0.0173\times M\times(5.867-p_a)-0.0014\times M\times(34-ta) \\ & -3.96\times10^{-8}\times f_{cl}\times[(t_{cl}+273)^4-(\overline{t}_r+273)^4-f_{cl}\times h_c(t_{cl}-t_a)\} \end{aligned} \tag{16}$$

where M is the rate of metabolic heat production, W/m2; tsk is the skin surface temperature, set at 33.5℃; to is room temperature, ℃;Icl is thermal resistance of clothing,set at 0.5clo;Ia/Icl is ratio of air layer thermal resistance to garment thermal resistance,set at 0.1 (m2·℃)/W.

III. C. TRNSYS Simulation Model

The library's HVAC system is modeled using TRNSYS, as illustrated in Figure. 7. It primarily consists of chillers, chilled water pumps, cooling pumps, cooling towers, air handling units (AHU), and fresh air units. The dark blue line represents the chilled water system, the red line indicates the cooling water system, the green line signifies the end fan coil loop, and the light blue line depicts the fresh air unit loop. The light green dotted line illustrates the trans-mission of the control and output signals.

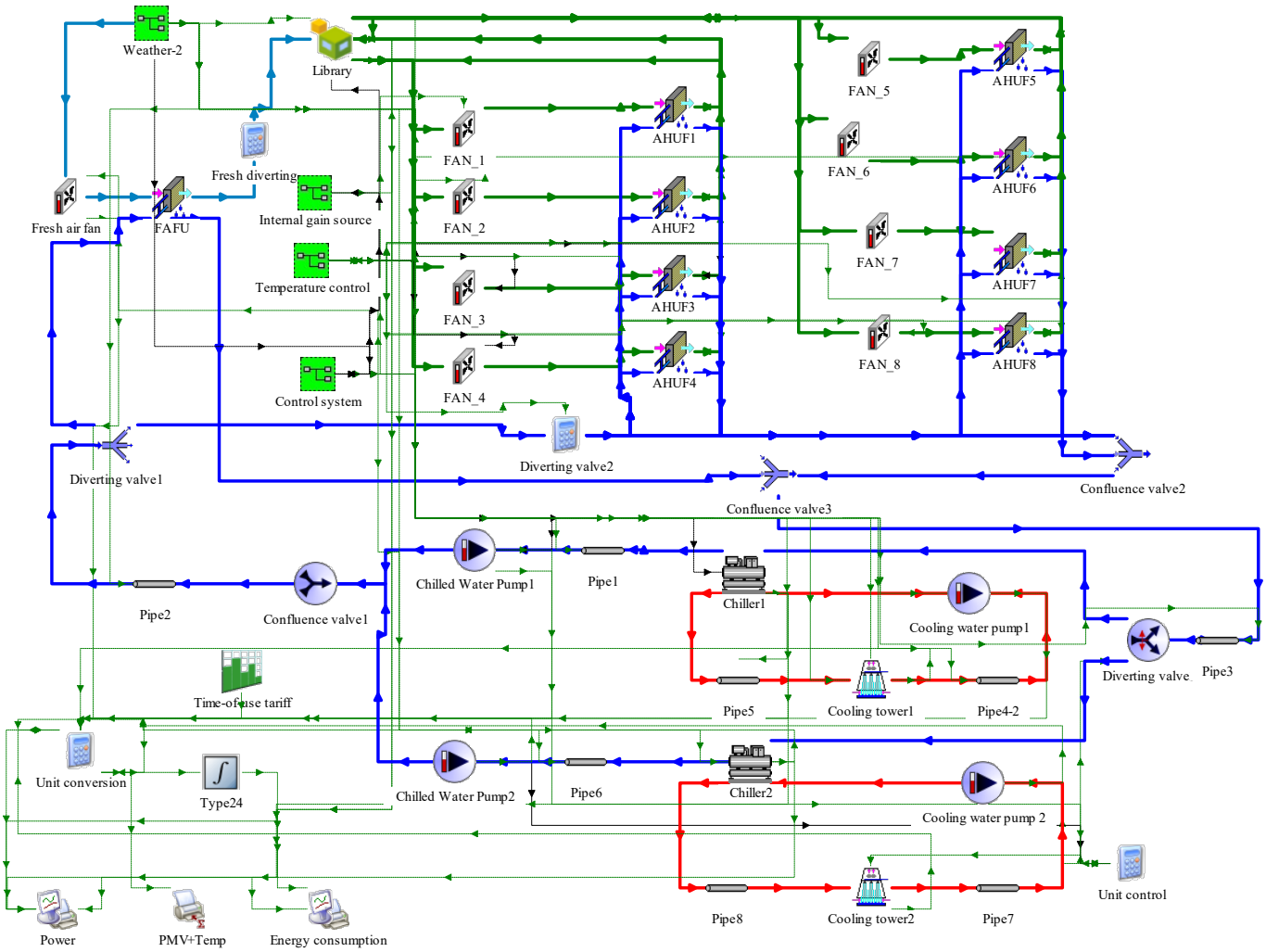

Figure 7: TRNSYS model of air conditioning system

III. D. Pre-processing inputs

This study utilizes weather data for Hengyang, sourced from the EnergyPlus website . Electricity pricing in Hengyang follows the time-of-use (TOU) tariff policy established by the China Southern Power Grid, which incentivizes users to optimize electricity consumption by shifting loads to off-peak hours, thereby alleviating peak demand pressure on the grid. The dynamic electricity pricing structure is illustrated in Figure 8, where the highest tariff of 0.94 CNY/(kW·h) applies during peak hours (8:30–11:30, 15:00–20:00), while the lowest tariff of 0.28 CNY/(kW·h) is in effect during off-peak hours (22:00–6:00, 22:00–24:00).

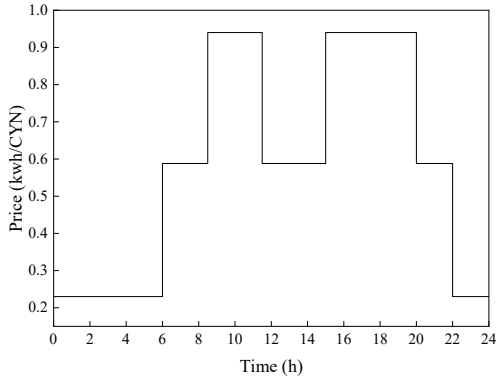

Figure 8: Time-of-use tariff in Hengyang city

IV. Multi-objective optimization model

A NSGA-II based-multi-objective optimization model considering energy flexibility, economic efficiency, and human thermal comfort is proposed in Figure 9. The objective functions, decision variables, constraints, and solution methodology are described in the following subsections.

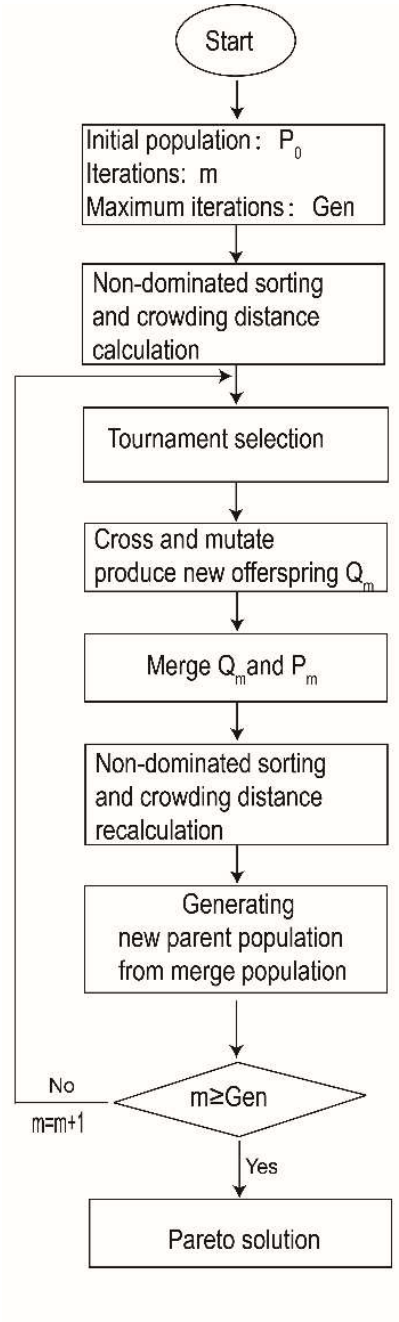

Figure 9: Flowchart of NSGA-Ⅱ

IV. A. Objective Function

Flexible load optimization scheduling involves multiple stakeholders, including electricity consumers, grid operators, and society at large. Electricity consumers are primarily concerned about their daily electricity bills, load management, and dissatisfaction arising from adjustments to air-conditioning temperature settings. Meanwhile, grid operators are focused on the impact of electricity consumption on the public grid. This paper aims to reconcile the needs of these diverse stakeholders as part of an optimization objective. The total operating cost throughout the day, human thermal comfort, and overall energy consumption have been established as the key objective functions.

Minimum daily electricity cost

$$C = \sum_{t=1}^{N} TOU \cdot P_{all}(t) \cdot \Delta t \tag{17}$$

where C represents the daily operating cost of the air-conditioning system, in CNY. TOU represents the time-of-day tariff, Δt is a time step denoting as 0.05 h. By implementing different electricity prices for different time periods, users are incentivized to shift their electricity consumption to low-cost periods and reduce demand during peak hours, thereby enhancing the overall flexibility and efficiency of the energy system.

Minimum daily energy consumption

$$\min E = \left(\begin{array}{l} \sum_{i=1}^{n} P_{chiler,i} + \sum_{i=1}^{m} P_{pump,i} + \sum_{i=1}^{k} P_{\mathrm{fan},i} \\ + \sum_{i=1}^{l} P_{coolingtower,i} \end{array} \right) \cdot t \tag{18}$$

where E represents the total energy consumption of the air-conditioning system; (kW·h); Pcoolingtower denotes the power of the cooling tower (kW) and is set to its rated value; t represents time (h).

Thermal comfort

$$\min \overline{PMV} = \min \frac{1}{n} \sum_{i=1}^{n} PMV_i \tag{19}$$

IV. B. Decision variables

In the terminal air handling unit, various types of fans are included, which can operate at variable frequencies to facilitate flexible energy consumption. Additionally, energy use can be adjustable based on the range of control parameters of indoor environmental. Practical adjustable parameters, such as indoor temperature, chilled water temperature, and fresh air flow, play a crucial role in optimizing the performance of HVAC systems. By fine-tuning these parameters, it is possible to achieve a good trade-off between energy efficiency and thermal comfort, thereby improving overall system performance and reducing operational costs. Since it is not practical to frequently change the temperature settings of central air conditioning, the scheduling interval for the temperature adjustments was established at one hour during the optimization process.

IV. C. Constraints

To ensure optimal system performance and effective dehumidification, the chilled water temperature should be maintained between 7°C and 12°C. The comfort specification indicates that the range of indoor temperature should be established between 24°C and 27.5°C.

The chilled water flow rate must remain within the specified limits, ensuring it neither drops below the minimum requirement nor exceeds the rated flow rate. The same principle applies to the cooling water flow rate, which should be maintained between 0.4 and 1 times the rated flow rate.

The maximum allowable indoor CO_2 concentration is set at 1200 ppm [20], [28]. A PID controller regulates the fresh air unit's speed to maintain this threshold. When the CO_2 concentration reaches 1200 ppm, the system automatically increases the volume of fresh air; conversely, as the concentration decreases, the fresh air supply is reduced. This dynamic regulation ensures indoor air quality while optimizing energy consumption, particularly during peak periods.

IV. D. The solution and decision-making method

This paper utilizes the NSGA-II optimization algorithm integrated within Jeplus software, a prominent tool for multi-objective optimization known for its effectiveness in addressing nonlinear problems characterized by discontinuities and local minima. In each iteration, a new population is generated through genetic operations, including selection, crossover, and mutation, progressively converging towards the optimal solution [24]. The parameter settings of the NSGA-II in this study include an initial population size of 80, a total of 800 iterations, a crossover probability of 0.9, and a mutation probability of 0.01.

he decision-making process integrates the Technique for Order of Preference by Similarity to Ideal Solution (TOPSIS) and the Shannon entropy method. Shannon entropy, proposed by Claude Shannon, is used to quantify the uncertainty of target attributes. A higher Shannon entropy value indicates greater data uncertainty and is typically used to reduce the weight of the corresponding objective [29], while a lower Shannon entropy value suggests more certain information, potentially assigning a higher $\overline{PMV}$ importance and substantial weight to the objective [30]. The final solution is evaluated using the TOPSIS method, which ranks alternatives based on their relative closeness to

the positive ideal and negative ideal solutions, selecting the alternative with the highest relative proximity closeness as the optimal solution. In this study, the TOPSIS method was implemented in the MATLAB environment.

The initial step involves creating a decision matrix:

$$r_{ij} = \frac{x_{ij}}{\sqrt{\sum_{i=1}^{m} x_{ij}^2}} \quad \forall j \tag{20}$$

where r_{ij} and x_{ij} are the elements of normalized and original decision matrix respectively.

The second step is to construct a weighted normalized decision matrix:

$$v_{ij} = r_{ij} * w_j \forall i, j \tag{21}$$

where w_j represents the weight assigned to attribute.

The third step involves identifying the ideal solution (A+) and the negative ideal solution (A-):

$$\begin{aligned} \mathrm{A}^{+} &= \{(\max_j v_{ij} \mid i \in I), (\min_j v_{ij} \mid i \in I'); \forall j\} = \{v_1^+, v_2^+, \ldots\} \\ \mathrm{A}^{-} &= \{(\min_j v_{ij} \mid i \in I), (\max_j v_{ij} \mid i \in I'); \forall j\} = \{v_1^-, v_2^-, \ldots\} \end{aligned} \tag{22}$$

where I and I' correspond to the benefit and cost attributes, respectively.

The fourth step is the calculation of separation measures: j

$$\begin{aligned} S_i^+ &= \sqrt{\sum_{i=1}^{n} (v_{ij} - v_i^+)^2} \forall j \\ S_i^- &= \sqrt{\sum_{i=1}^{n} (v_{ij} - v_i^-)^2} \forall j \end{aligned} \tag{23}$$

The fifth step involves calculating the relative closeness to the ideal solution:

$$C_j^+ = \frac{S_j^+}{S_j^+ + S_j^-} \tag{24}$$

The final step involves sorting the optimal solution based on the C_j^+ values.

IV. E. Performance of demand response under various strategies

To compare and validate the performance of the proposed optimization strategy, the following simulation control groups have been established. July 8th has been selected as a representative summer day for analysis.

Table 4: Simulation strategy settings

Strat-egy	Practical method for accomplishing a task.
ST1	The temperature remained constant at 25°C throughout the day, while the chilled water was maintained at a steady 7°C.
ST2	Fresh air unit PID control
ST3	Individual optimization of indoor temperature strategies based on genetic algorithms
ST4	Individually optimized room temperature strategy and fresh air unit PID control
ST5	Genetic algorithm strategy for simultaneous optimization of chilled water supply temperature and room temperature
ST6	Genetic algorithm for simultaneous optimization of chilled water supply temperature and room temperature and fresh air unit PID control

Table 4 presents the baseline conditions for ST1, where the ambient temperature is maintained at a constant 25°C, and the chilled water temperature remains at 7°C throughout the day. The analysis compares indoor temperature, air conditioning energy consumption, costs, and thermal comfort on a typical day under different control strategies. Among the six control strategies examined, all parameters remain consistent except for indoor temperature, chilled water supply temperature, and fresh air blower speed.

V. Results and analyses

V. A. Optimization results

Figure 10 illustrates the settings of optimal indoor temperature. To achieve better control, the ST3 to ST6 strategies utilize a genetic algorithm. This approach aims to balance comfort, energy consumption, and electricity costs, thereby achieving the dynamic optimal value. The analysis results indicated that, the air conditioning setpoint temperature mainly ranges from 26°C to 27.5°C, with the majority of DR intervals maintaining a setpoint of 27.5°C during the DR periods under the ST3 to ST6 strategies. Conversely, , the temperature setpoint generally falls within 23°C to 25.5°C during non-DR periods, with a specific indoor temperature setting of 23°C to 24°C at 13:00, Then the temperature gradually increase. This pre-cooling strategy is implemented before the second DR period(15:00~20:00) to dissipate residual indoor heat and humidity in advance, which can effectively reduce electricity consumption during the upcoming DR event. Additionally, the settings of temperature in the ST6 strategy are significantly lower than those in other strategies. This is primarily due to the multi-objective optimization, which accounts for various factors such as air conditioning system load, chiller efficiency, fresh air unit performance, and indoor air quality, leading to relatively lower indoor temperature setpoints. Based on the above analysis, it can be concluded that the NSGA-II algorithm can effectively distinguishes peak electricity demand periods and regular periods.

The optimized results indicated that Maintaining a higher supply water temperature under low-load operation is beneficial for energy savings and reducing equipment wear. when the chiller's part load ratio (PLR) is less than or equal to 0.3 and the supply water temperature is set to 12.125°C. a lower supply water temperature can more effectively meet cooling demands while maintaining system efficiency, when the part load ratio reaches 1,and the supply water temperature is set to 9.5°C. Under high-load conditions, The detailed results are presented in Table 5.

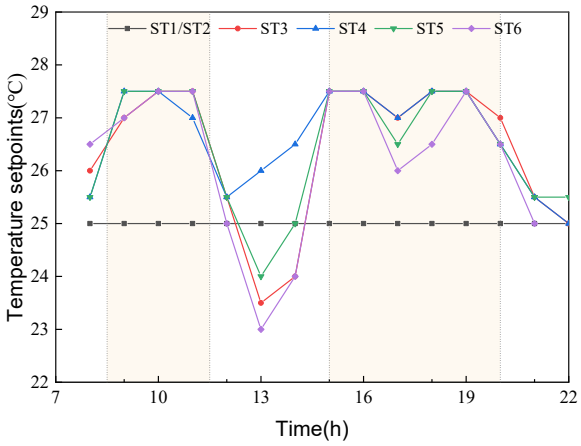

Figure 10: Indoor temperature setpoint

Table 5: Chilled water temperature Settings

Partial load rate(%)	Original chilled water temperature(℃)	Optimized chilled water temperature(℃)
⩽30	7	12.125
40	7	11.75
50	7	11.375
60	7	11
70	7	10.625
80	7	10.25
90	7	9.9875
100	7	9.5

V. B. Different simulation strategies for DR

This section assesses the impact of the four proposed experimental strategies by analyzing room temperature, predicted mean vote (PMV), indoor CO2 concentration electricity consumption, and operational costs.

Figure 11 illustrates the comparison of actual operating temperatures under the six implemented strategies. , It can be seen that the actual operating temperature significantly exceeds the setpoint during the first hour. This phenomenon is primarily attributed to the thermal storage capacity of the building envelope, the large indoor space, and occupant movement. During the remaining periods, the temperature fluctuates in response to variations in

indoor conditions and setpoint adjustments. The final temperature consistently fluctuates within a ±0.5°C range. This indicates that the strategies from ST3 to ST6 can effectively reduce peak power consumption while meeting cooling requirements.

Figure 12 illustrates the variations in indoor temperature and PMV over time under different strategies. The PMV values for all strategies stay between 0 and 1, to ensure thermal comfort, except for the first half-hour after system startup. The comparison between ST2 and ST3 indicates that adjusting the fresh air volume has minimal impact on thermal comfort, whereas changes in indoor temperature significantly affect the PMV index The indoor temperature under the ST1 strategy fluctuates between 24.87℃ and 25.84℃with PMV values ranging from 0.21 to 0.333, meet the thermal comfort requirements for occupants once the conditioning system is activated., The indoor temperature generally ranges from 26.58℃ to 27.71℃ during the first DR period in the optimized strategies ST3–ST6 with PMV values varying between 0.21 and 0.96., the indoor temperature fluctuates between 23.8℃ and 25.21℃ during normal periods (13:00–15:00), while the PMV values remain within 0.11 to 0.32. It can be observed that, PMV values remain below 1with its fluctuating within the range of 0 to 1 under ST3–ST6 strategies, indicating a good level of indoor thermal comfort. Only under the ST5 and ST6 strategies do PMV values approach 1, essentially meeting the thermal comfort requirements for occupants. It was found that the ST3–ST6 strategies appropriately increased heat retention and thermal load while achieving an acceptable balance in indoor thermal comfort during DR periods.

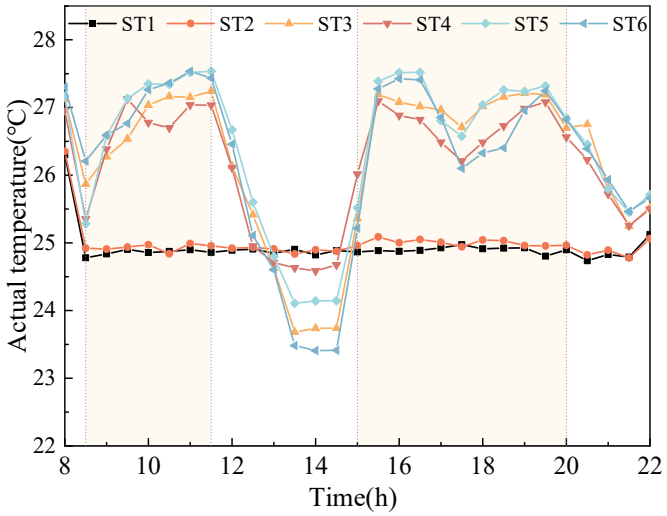

Figure 11: Room actual temperature

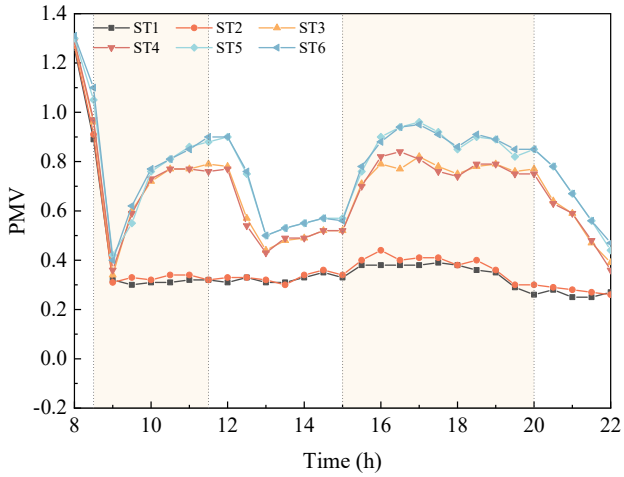

Figure 12: PMV

V. C. Indoor CO2 concentration

Figure 13 presents a comparison of indoor CO_2 concentrations under six different strategies. This strategy aims to maintain indoor CO_2 concentrations below the maximum threshold of 1200 ppm. The fluctuations in the CO_2

concentration bar chart are closely correlated with occupancy rates, illustrating the process of using PID control to regulate the rotational speed of the fresh air unit. The highest recorded indoor CO_2 concentration was 924.45 ppm before the intervention, whereas the concentration stabilized at approximately 1130 ppm after implementing the strategy, which can effectively reducee energy demand during periods of low occupancy and dynamically adjusts airspeed during high-load periods to meet indoor air quality requirements. This approach alleviates the pressure on the power grid while ensuring users' comfort, serving as a practical reference for demand-response air-conditioning systems.

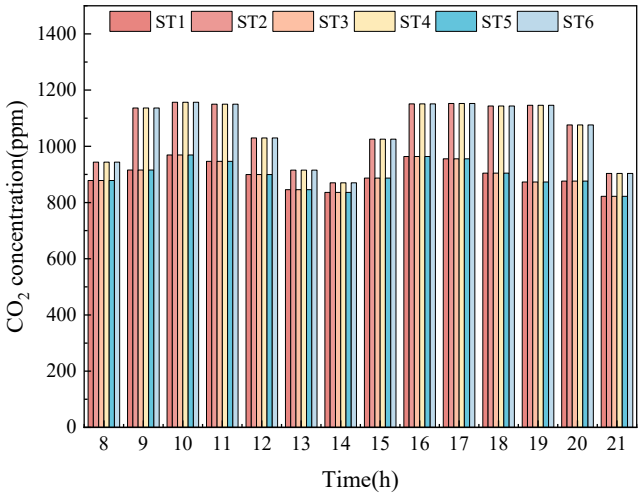

Figure 13: Indoor carbon dioxide concentration

V. D. Air-conditioning energy consumption and operating costs

To further evaluate of the ST6 strategy's performance in energy savings and cost reduction, the energy consumption and electricity costs under different strategies is compared, as shown in the figures.

As illustrated in Figure 14 and Figure 15, the optimization effects of the six demand response (DR) strategies are progressively improved, with the overall energy consumption and electricity costs decreasing sequentially from ST2 to ST6. Among them, the ST6 strategy demonstrates the highest control efficiency, which achieves an energy reduction of 1195.58 kWh during the DR period, corresponding to an energy savings rate of approximately 34.30%. This reduction in energy consumption results in electricity cost savings of $1123.84, achieving a 34.30% of energy saving. The total daily energy savings rate reaches up to 14.92%, while the operational cost is saved 20.00%.

The difference in energy consumption primarily origins from the variable frequency control of the fresh air system between the ST1 and ST2 strategies, as both occupant presence and fresh air intake serve as major sources of latent heat load. However, the DR effect is constrained by indoor occupancy and air quality constraints, resulting in energy reduction of 268.68 kWh and cost savings of 251.39 CNY. The difference in energy consumption and costs lies in the air-conditioning system's thermal load response between the ST3 and ST2 strategies. As the buildings possess thermal storage capacity, the air-conditioning system can pre-cool the indoor environment to, store cold or heat energy in advance. This strategy extends the temperature buffering period, which allows operate in low-load mode during peak hours of electricity pricing and facilitate load shifting from peak to off-peak periods. In contrast, the fresh air system has a relatively weaker load-shifting capability due to the inability of storage of CO_2, resulting in a shorter buffering period. The ST3 strategy achieves an additional peak energy consumption reduction of 309.61 kWh compared to the ST2.

The ST4 strategy incorporates dynamic indoor temperature settings and variable frequency control of the fresh air system amd integrates the advantages of ST1, ST2, and ST3., The ST4 strategy, solely relying on indoor temperature resetting, saves an additional 187.47 kWh of DR energy consumption and 410.84 CNY in daily operational costs compared to ST3. The distinction between ST5 and ST3 lies in the dual optimization strategy that combines indoor temperature settings for different electricity pricing periods with the optimal chilled water supply temperature based on corresponding part-load ratios. This approach enhances the coefficient of performance (COP) of the chiller, leading to saving of energy consumption. Compared to ST3, the ST5 strategy can result in a reduction in power consumption of 406.25 kWh and in operational costs of 381.87 CNY during the DR period, while achieving an overall reduction of daily energy of 337.94 kWh and a cost saving of 341.85 CNY.

Based on advantages of ST1, ST2, ST3, ST4, and ST5, the ST6 strategy integrates the indoor temperature settings, chilled water supply temperature, and fresh air unit control across different electricity pricing periods. This strategy enhances the energy efficiency and demand response capability of the air-conditioning system through a triple optimization strategy. Based on the above analysis, it can be concluded that the ST6 is undoubtedly the optimal control strategy due to its advantages of taking improvements in energy efficiency, cost reduction, demand response capability, and system flexibility into consideration, The ST6 strategy enables precise regulation of each subsystem within the air-conditioning system, minimizing energy consumption and costs while ensuring thermal comfort and effectively responding to grid demand response requirements.

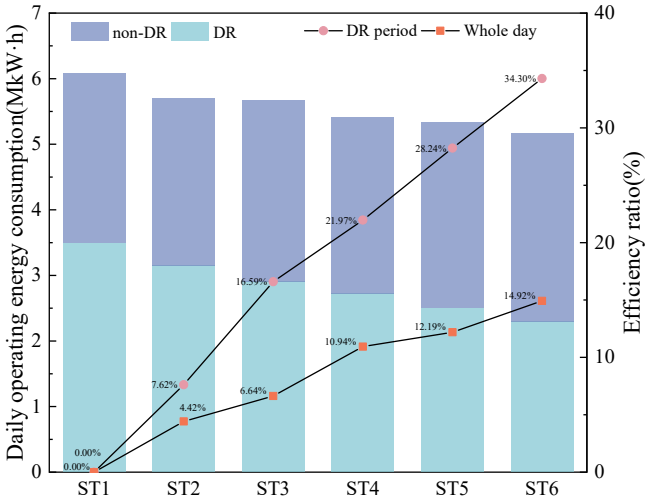

Figure 14: Air conditioning system daily operating energy consumption

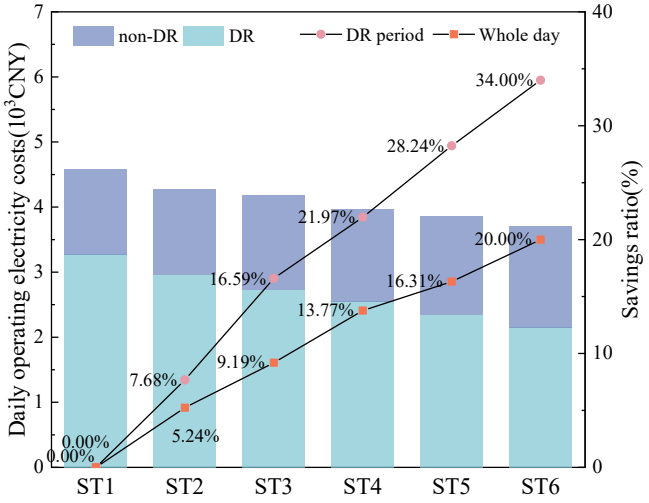

Figure 15: Air conditioning system daily operating cost

V. E. DR effect performance in buildings with different occupant densities

The variation in occupant density across different floors significantly affects the cooling load of the building. Therefore, different occupant densities are assumed to evaluate the effect of potential cooling loads on the performance of the ST6 strategy. The implementation effectiveness is simulated under maximum library attendance scenarios of 2,793, 2,318, 1,756, and 1,249 individuals of the ST6 strategy. Two seating arrangements are considered. Take an actual attendance of 1,756 individuals as an example, these occupants may either be evenly distributed across floors 1 to 8 or concentrated on floors 1 to 6,with only brief occupancy on floors 7 and 8, which can be regarded as a short stay. Scenario 1 assumes that occupants are evenly distributed across all floors, while Scenario 2 assumes that they are concentrated on specific floors, allowing air conditioning on unoccupied floors to be turned off. Table 6 presents the hierarchical control strategies corresponding to different occupancy scenarios.

Table 6: Hierarchical control strategies

Actual attendance	Scenario 1		Scenario 2	
	Opening floor	Floor occupancy rates	Opening Floor	floor occupancy rates
2793	1-8	1	1-8	1
2318	1-8	0.83	1-7	0.927
1756	1-8	0.76	1-6	0.87
1249	1-8	0.44	1-5	0.77

V. E. 1) Uniform distribution of indoor occupants

Figure 16 and Figure 17 illustrate the simulated daily operational energy consumption and electricity costs under different attendance conditions for the ST6 strategy, The study indicates that as the maximum library attendance decreases, the ST6 strategy exhibits significantly enhanced flexibility in load regulation during the demand response (DR) phase. Specifically, energy-saving rates are 34.30%, 37.22%, 39.63%, and 42.41% for different attendance levels during the DR phase, while the electricity cost savings of overall daily are 19.20%, 21.67%, 23.35%, and 25.44%, respectively. This trend is primarily attributed to the load reduction of air-conditioning, the demand decrease of fresh air, minimized impact of load curtailment, and improved efficiency of the chilled water system.

Firstly, a reduction in attendance directly lead to the decrease of the cooling load of the air-conditioning system, including reductions in both sensible and latent heat loads. This enables the cooling source system to scale back cooling supply, thereby lowering refrigeration energy consumption. Additionally, a lower indoor occupant density results in reduced CO_2 generation, which decreases the demand for fresh air. Consequently, the operation time and airflow supply of the fresh air unit can be further optimized, leading to a reduction in the energy consumption required for fresh air processing. Furthermore, when attendance is high, reducing the air-conditioning load may cause indoor temperatures to rise too quickly, potentially compromising occupant comfort. However, temperature fluctuations occur more gradually under conditions of low occupant density. This ensures that even with a greater reduction in cooling load, indoor thermal comfort remains largely unaffected.

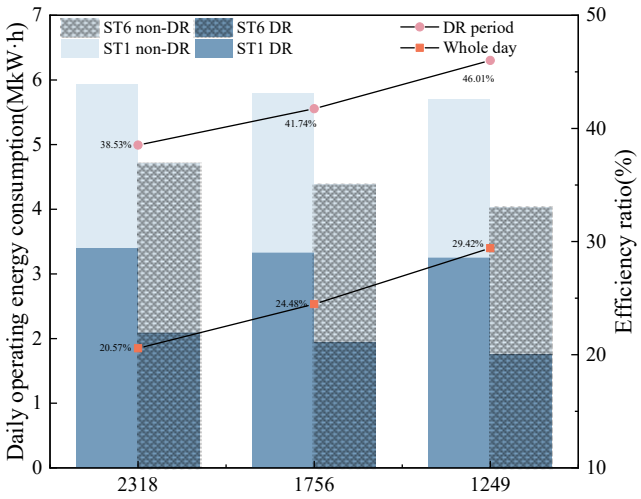

Figure 16: Energy consumption under different visitor numbers

V. E. 2) Indoor occupants concentrated in specific areas

The previous section has confirmed that lower occupant density enables the air-conditioning system to curtail more load during the demand response (DR) period. To further assess the effect of different seating arrangements on demand response (DR) potential, Figure 18 and Figure 19 illustrate the comparison of daily operational energy consumption and electricity costs under two scenarios (uniform distribution and concentrated distribution) at varying occupant densities.

The study reveals a consistent trend in DR load reduction across different occupant densities, indicating that the potential for DR load curtailment increases significantly as occupant density decreases.

A detailed analysis indicates that when the library attendance drops to 2,318 people, Scenario 2 (concentrated distribution) achieves a DR-phase energy reduction of 74.98 kWh, accounting for 3.5% of the total DR-period energy consumption. Meanwhile, the energy savings of full-day reach 254.57 kWh, or 5.13% of the total energy consumption. However, as the attendance of people further declines to 1,249, the reducible DR-phase energy consumption

increases significantly to 300.35 kWh, representing 15.63% of the total DR-period energy consumption, while full-day energy savings rise to 681.05 kWh, or 14.62% of total energy consumption. This reduction trend in energy consumption is mirrored in daily operational costs.

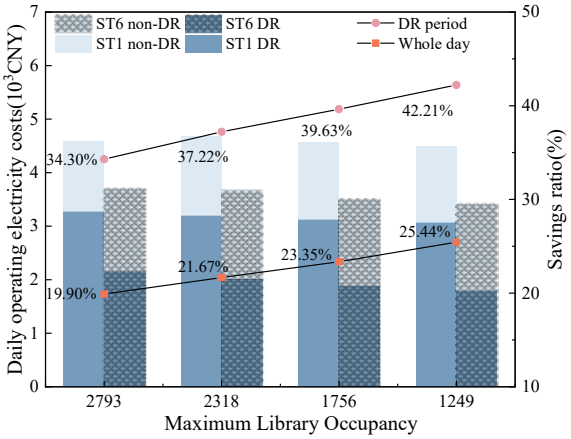

Figure 17: Electricity cost under different visitor numbers

As shown as Table 7, compared to Scenario 1, Scenario 2 achieves a DR-phase electricity cost reduction of 70.48 CNY when attendance is at 2,318 people, accounting for 3.5% of the total DR-period electricity costs. However, when attendance drops to 1,249 people, DR-phase electricity cost savings surge to 185.06 CNY, representing 10.2% of total DR-period electricity costs. Similarly, full-day electricity cost savings increase significantly, rising from 175.98 CNY (4.79%) to 469.65 CNY (13.76%).

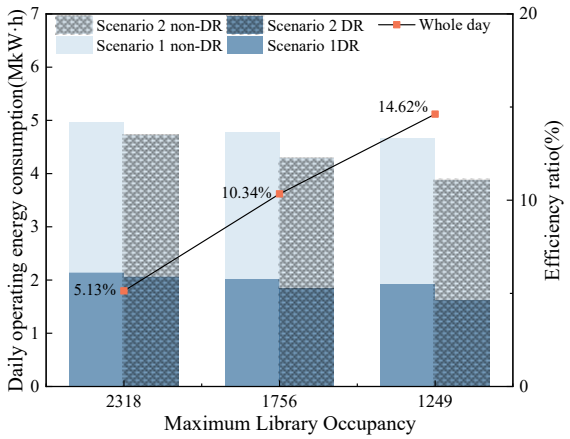

Figure 18: Comparison of energy usage in two scenarios

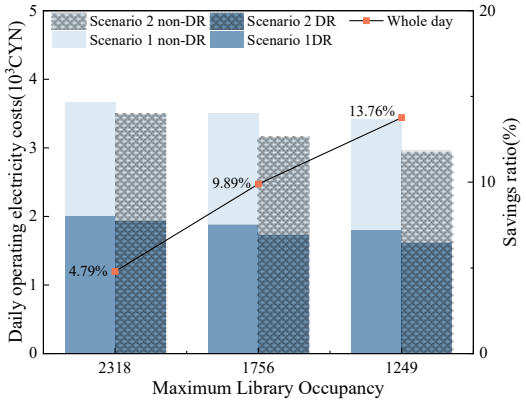

Figure 19: Comparison of electricity costs in two scenarios

Concentrated occupant distribution proves to be more effective than uniform distribution in enhancing potential DR load curtailment and energy savings. Firstly, concentrated distribution minimizes unnecessary cooling areas. The concentrated distribution allows air-conditioning systems on unoccupied floors to be partially or fully turned off, which eliminates redundant energy consumption. In contrast, uniform distribution necessitates operation across all floors resulting in unnecessary energy consumption. Additionally, load concentration enables chillers and fans to function more efficiently, preventing performance declines caused by low-load operation and improving the system's coefficient of performance (COP). Secondly, reduced fresh air demand further decreases energy consumption. Under uniform distribution, fresh air supply must be maintained throughout the entire building, whereas concentrated distribution limits fresh air requirements to occupied areas, reducing the energy needed for fresh air processing. Furthermore, concentrated distribution allows for more flexible load adjustment, enhancing DR load curtailment capability. In a uniform distribution scenario, substantial load reductions can compromise occupant comfort. However, with concentrated distribution, air-conditioning systems in unused areas can be directly shut down, enabling greater load reductions while maintaining a comfortable indoor environment more effectively.

Table 7: Rates of energy and electricity costs for Scenarios 1 compared to Scenario 2

Attendance	DR energy	Whole energy	DR electricity costs	Whole electricity costs
2318	40 kW·h (1.88%)	210 kW·h (4.27%)	30 CNY (1.5%)	140 CNY (3.31%)
1756	50 kW·h (2.51%)	310 kW·h (6.61%)	50 CNY (2.67%)	180 CNY (6.07%)
1249	164kW·h(8.33%)	580 kW·h (12.58%)	150 CNY (8.33%)	400 CNY (11.83%)

VI. Discussion

This strategy can assist demand response (DR) in coordinating various subsystems of air conditioning systems to meet the grid's peak demand while maintaining indoor temperature and air quality. Additionally, the building's thermal inertia is one of several factors that affects its energy flexibility. The pre-cooling system can successfully shift electricity usage during peak hours even with the most effective control strategy, thereby reducing the energy consumption of the air conditioning units and enhancing the building's flexibility. Future studies could be focused on the investigation the optimal pre-cooling duration and timing for different attendance. Meanwhile, the algorithmic accuracy and iteration speed of multi-objective optimization can be improved by implementing more advanced algorithms.

VII. Conclusions

This section is not mandatory but can be added to the manuscript if the discussion is unusually long or complex.

This paper proposes a multidimensional synergistic optimization strategy based on load DR across different electricity pricing periods taking into the comprehensive effect of indoor temperature settings, chilled water supply temperature, and fresh air unit control consideration. The effectiveness of this strategy is validated through comparisons with a single optimized indoor temperature control strategy and a strategy that concurrently optimizes both indoor temperature and chilled water supply temperature. The primary conclusions are outlined as follows:

To achieve optimal system performance, the multi-dimensional synergistic load optimization control strategy takes into account all-day energy consumption, time-of-use tariffs, and comfort requirements. It accomplishes this by automatically optimizing indoor temperature and chilled water supply temperature, while also adjusting the speed of the fresh air unit as necessary. The performance is superior across all metrics, achieving a 34.30% reduction in energy consumption during the demand response (DR) phase, a 14.92% decrease in total daily energy consumption, and a 20.00% reduction in overall daily operational costs. These results demonstrate the feasibility and effectiveness of the proposed strategy in reducing peak loads, conserving energy, and ensuring occupant comfort.

The strategy's flexibility increases as the library attendance declines, with the ST6 strategy achieving 41.10% flexible regulation potential when attendance drops to 1,249 people.

Centralized occupant distribution enhances the ST6 strategy, outperforming uniform distribution. Under favorable DR conditions, ST6 achieves a 46.1% DR-phase energy reduction and 33.92% electricity cost savings when attendance is 1,249, highlighting the significant flexibility benefits of varying occupancy.

Author Contributions

Methodology, Zehua Liu and Tianhui Yang;software, Tianhui Yang; validation, Chen Yuan; formal analysis, Tianhui Yang; investigation, Dan Xie; resources, Dan Xie; data curation, Bin Wang; writing—original draft preparation, Tianhui Yang; writing—review and editing, Tianhui Yang; visualization, Tianhui Yang; supervision, Tianhui Yang; project administration, Zehua Liu; funding acquisition, Zehua Liu. All authors have read and agreed to the published version of the manuscript.

Institutional Review Board Statement
Not applicable.

Informed Consent Statement
Not applicable.

Data Availability Statement
We encourage all authors of articles published in MDPI journals to share their research data. In this section, please provide details regarding where data supporting reported results can be found, including links to publicly archived datasets analyzed or generated during the study. Where no new data were created, or where data is unavailable due to privacy or ethical restrictions, a statement is still required. Suggested Data Availability Statements are available in section “MDPI Research Data Policies” at https://www.mdpi.com/ethics.

Conflicts of Interest
The authors declare that they have no known competing financial interests or personal relationships that could have appeared to influence the work reported in this paper.

Abbreviations
The following abbreviations are used in this manuscript:

DR	Demand response
PMV	Predicted mean vote

References
[1] Ruan, Y.; Ma, J.; Meng, H.; Qian, F.; Xu, T.; Yao, J., Potential quantification and impact factors analysis of energy flexibility in residential buildings with preheating control strategies. Journal of Building Engineering 2023.
[2] Meng, Q.; Li, Y.; Ren, X.; Xiong, C.; Wang, W.; You, J., A demand-response method to balance electric power-grids via HVAC systems using active energy-storage: Simulation and on-site experiment. Energy Reports 2021, 7, 762-777.
[3] Niu, J.; Tian, Z.; Lu, Y.; Zhao, H., Flexible dispatch of a building energy system using building thermal storage and battery energy storage. Applied Energy 2019, 243, 274-287.
[4] Hwang, H.; Yoon, A.; Yoon, Y.; Moon, S., Demand response of HVAC systems for hosting capacity improvement in distribution networks: A comprehensive review and case study. Renewable and Sustainable Energy Reviews 2023, 187, 113751.
[5] Sánchez Ramos, J.; Pavón Moreno, M.; Guerrero Delgado, M.; Álvarez Domínguez, S.; F. Cabeza, L., Potential of energy flexible buildings: Evaluation of DSM strategies using building thermal mass. Energy and Buildings 2019, 203, 109442.
[6] Hoyt, T.; Arens, E.; Zhang, H., Extending air temperature setpoints: Simulated energy savings and design considerations for new and retrofit buildings. Building and Environment 2015, 88, 89-96.
[7] Li, Z.; Meng, Q.; Wei, Y. a.; Zhang, L.; Sun, Z.; Lei, Y.; Yang, L.; Yan, X., Dynamic room temperature setpoints of air-conditioning demand response based on heat balance equations with thermal comfort model as constraint: On-site experiment and simulation. Journal of Building Engineering 2023, 65, 105798.
[8] Wang, J.; Wei, Z.; Zhu, Y.; Zheng, C.; Li, B.; Zhai, X., Demand response via optimal pre-cooling combined with temperature reset strategy for air conditioning system: A case study of office building. Energy 2023, 282, 128751.
[9] Li, Z.; Sun, Z.; Meng, Q.; Wang, Y.; Li, Y., Reinforcement learning of room temperature set-point of thermal storage air-conditioning system with demand response. Energy and Buildings 2022, 259, 111903.
[10] Li, Z.; Wang, P.; Zhang, J.; Mu, S., A strategy of improving indoor air temperature prediction in HVAC system based on multivariate transfer entropy. Building and Environment 2022, 219, 109164.
[11] Huang, S.; Katipamula, S.; Lutes, R., Experimental investigation on thermal inertia characterization of commercial buildings for demand response. Energy and Buildings 2021, 252, 111384.
[12] Wang, H.; Wang, S.; Tang, R., Development of grid-responsive buildings: Opportunities, challenges, capabilities and applications of HVAC systems in non-residential buildings in providing ancillary services by fast demand responses to smart grids. Applied Energy 2019, 250, 697-712.
[13] Christantoni, D.; Oxizidis, S.; Flynn, D.; Finn, D. P., Implementation of demand response strategies in a multi-purpose commercial building using a whole-building simulation model approach. Energy and Buildings 2016, 131, 76-86.
[14] Ran, F.; Gao, D.-c.; Zhang, X.; Chen, S., A virtual sensor based self-adjusting control for HVAC fast demand response in commercial buildings towards smart grid applications. Applied Energy 2020, 269, 115103.
[15] Dai, M.; Li, H.; Wang, S., Event-driven demand response control of air-conditioning to enable grid-responsive buildings. Automation in Construction 2023, 150, 104815.
[16] Wang, S.; Tang, R., Supply-based feedback control strategy of air-conditioning systems for direct load control of buildings responding to urgent requests of smart grids. Applied Energy 2017, 201, 419-432.
[17] Vand, B.; Martin, K.; Jokisalo, J.; Kosonen, R.; Hast, A., Demand response potential of district heating and ventilation in an educational office building. Science and Technology for the Built Environment 2020, 26, (3), 304-319.
[18] Rotger-Griful, S.; Jacobsen, R. H.; Nguyen, D.; Sørensen, G., Demand response potential of ventilation systems in residential buildings. Energy and Buildings 2016, 121, 1-10.

[19] Ma, Z.; Cui, S.; Chen, J., Demand response through ventilation and latent load adjustment for commercial buildings in humid climate zones. Applied Energy 2024, 373, 123940.
[20] Luo, Z.; Zhang, J.; Zhang, T.; Liu, X., Potential Evaluation and Influencing Factors of Fresh Air System Demand Response. Power System Technology 2024, 48, (07), 775-2783.
[21] Li, Z.; Meng, Q.; Wei, Y. a.; Yan, X.; Lei, Y.; Wu, X.; Liu, J.; Wang, L., Reinforcement learning-based demand response strategy for thermal energy storage air-conditioning system considering room temperature and humidity setpoints. Journal of Energy Storage 2023, 72, 108742.
[22] Wang, H.; Ding, Z.; Tang, R.; Chen, Y.; Fan, C.; Wang, J., A machine learning-based control strategy for improved performance of HVAC systems in providing large capacity of frequency regulation service. Applied Energy 2022, 326, 119962.
[23] Yuan, J.; Xiao, Z.; Chen, X.; Lu, Z.; Li, J.; Gang, W., A Temperature & Humidity Setback Demand Response Strategy for HVAC Systems. Sustainable Cities and Society 2021, 75, 103393.
[24] Wang, P.; Liu, Z.; Chen, D.; Li, W.; Zhang, L., Experimental study and multi-objective optimisation of a novel integral thermoelectric wall. Energy and Buildings 2021, 252, 111403.
[25] Xu, W.; Zou, Y.; Chen, X.; Sun, D., National Standard “Design Standard for Energy Efficiency of Public Building” GB50189-2015. Construction Science and Technology 2018, 0, (16), 39-45.
[26] Southard, L. E.; Liu, X.; Spitler, J. D., Performance of HVAC systems at ASHRAE HQ. Ashrae Journal 2014, 56, (12), 12-23.
[27] Li, H.; Hu, H.; Wu, Z.; Kong, X.; Fan, M., Modified predicted mean vote models for human thermal comfort: An ASHRAE database-based evaluation. Renewable and Sustainable Energy Reviews 2025, 209, 115042.
[28] Zhang, T.; Liu, X.; Liu, X., Reunderstanding of air conditioning system from perspective of new power system. Heating Ventilating & Air Conditioning 2023, 53, (8), 13-21.
[29] Li, M.; Mu, H.; Li, N.; Ma, B., Optimal design and operation strategy for integrated evaluation of CCHP (combined cooling heating and power) system. Energy 2016, 99, 202-220.
[30] Jing, R.; Zhu, X.; Zhu, Z.; Wang, W.; Meng, C.; Shah, N.; Li, N.; Zhao, Y., A multi-objective optimization and multi-criteria evaluation integrated framework for distributed energy system optimal planning. Energy Conversion and Management 2018, 166, 445-462.